THE JOURNAL OF PHYSICAL CHEMISTRY C
A JOURNAL OF THE AMERICAN CHEMICAL SOCIETY

pubs.acs.org/JPCC

Article

Double Ag Nanowires on a Bilayer MoS_2 Flake for Surface-Enhanced Raman Scattering

Lulu Yu, Liu Lu,* Linghui Zeng, Xiaohong Yan, Xifeng Ren, and Judy Z. Wu*

Cite This: *J. Phys. Chem. C* 2021, 125, 1940−1946

Read Online

ACCESS | Metrics & More | Article Recommendations

ABSTRACT: Surface-enhanced Raman spectroscopy (SERS) of rhodamine 6G (R6G) was investigated using a hybrid nanostructure of double-aligned Ag nanowires (AgNWs) on a bilayer triangular MoS_2 flake under excitation of polarized light. Enhanced R6G Raman signatures were achieved on the hybrid AgNWs−MoS_2 SERS substrates as compared to the AgNWs-only ones. Moreover, the polarization has been found to affect not only the Raman intensities of R6G and MoS_2 on both SERS substrates but also the R6G Raman enhancement factor on the hybrid AgNWs−MoS_2 SERS substrate. Specifically, this enhancement was found to be the largest (lowest) when the polarization is perpendicular (parallel) to the axial direction of the aligned AgNWs. In addition, a theoretical simulation has revealed that the SERS enhancement by the MoS_2 in the hybrid AgNWs−MoS_2 SERS substrates is primarily attributed to the enhanced evanescent electric field of the hot spot at the interface between AgNWs and MoS_2.

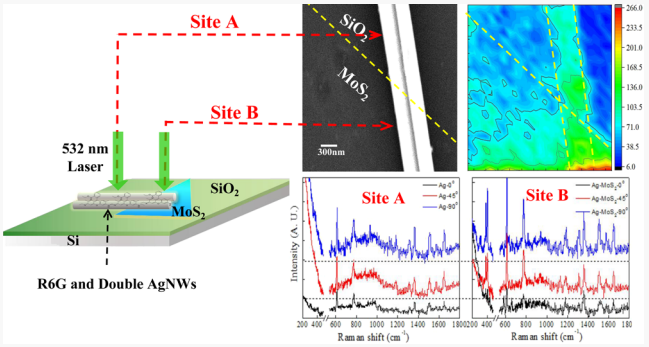

1. INTRODUCTION

The composition system of two-dimensional molybdenum disulfide (MoS_2) and metallic nanostructures has attracted more and more attention because this combination has brought many amazing phenomena. For example, the Au−graphene−MoS_2 composition structure has significantly improved the sensitivity of biosensor relative to the Au or Au−graphene structure.[1] The coupling of metal and MoS_2 can selectively enhance the specific excitons' fluorescence and the temperature of MoS_2.[2,3] Besides, this coupling is also found to improve the light response speed and photocurrent of transition metal dichalcogenide optoelectronic devices,[4,5] as well as the photocatalytic and electrocatalytic ability of MoS_2.[6,7]

Similarly, research on surface-enhanced Raman spectroscopy (SERS) also paid attention to the introduction of MoS_2 nanostructures to the conventional SERS substrate. As a Raman enhancement technology, it is known that SERS can enhance the intensity of the Raman signature peaks of molecules and therefore provide a promising method for the realization of biosensing with single molecule sensitivity.[8−13] So far, researchers have conducted in-depth studies on the preparation of various metals and MoS_2 hybrid structure and showed the superior properties of this structure as an active SERS substrate. Su et al. prepared a MoS_2-coated Au NP composite structure by an in situ method and showed high-quality SERS activity of this structure.[14] Qiu et al. modified MoS_2 microspheres with cauliflower-like Au NPs arrays and used it for in situ molecular detection and proved that it can be an efficient molecular detector by identifying 10^{-14} M rhodamine 6G (R6G) or methylene blue under different laser wavelength excitations.[15] Similarly, Achintya found that a hybrid structure of MoS_2 nanoflowers and Au NPs not only can detect R6G probe molecules at concentrations as low as 10^{-12} M but also have high sensitivity and good reproducibility in high-level (10^{-3} M) bilirubin detection.[16] Chen fabricated a MoS_2-coated Ag NP hybrid system for SERS; the minimum detected concentration of this hybrid system for R6G can reach 10^{-9} M, which is 1 order of magnitude lower than that for Ag NPs.[17] Besides, Zu et al. demonstrated that photo-excited excitons can effectively change the optical response of the MoS_2 monolayer and can be used to actively control surface plasmon resonance (SPR) in MoS_2−Ag hybrid nanostructures.[18]

However, most of the previous research studies are focused on SERS over a large sample area with many MoS_2 NPs and metal NPs, which prevents the study the SERS mechanism of this hybrid structure at a microscopic scale associated with one

Received: September 8, 2020
Revised: January 4, 2021
Published: January 19, 2021

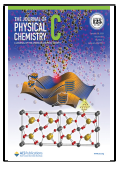

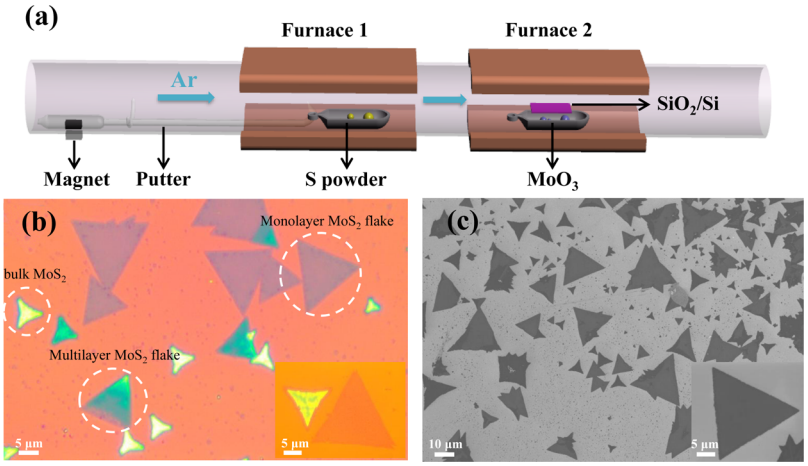

Figure 1. (a) Schematic of the experimental setup for the CVD growth of MoS_2 flakes. (b) Optical images of MoS_2 obtained by CVD. (c) SEM morphology of a representative MoS_2 flake.

or few involving nanostructures. Moreover, the so-called "hot spot" plays a dominant role in SERS performance that has been found to be dependent on the incident light polarization.[19] Therefore, it is necessary to investigate the SERS performance of the MoS_2 and Ag hybrid system under different incident light polarization at a microscopic scale.

In this work, a hybrid nanostructure of double Ag nanowires (AgNWs) on a bilayer MoS_2 flake was adopted for an investigation of the SERS of R6G probe molecules when the incident light polarization angle was varied with respect to axis of the AgNWs to systematically alter the SERS coupling between the AgNWs and MoS_2 flake. The experimental comparison of the same double-aligned AgNWs on the silica substrate and MoS_2 flake, as well as the simulation results demonstrated the superiority of the Ag/MoS_2 hybrid on SERS performance was caused by the electric field hot spot at the interface between Ag and MoS_2. Besides, the SERS performance of the hybrid structure versus the angle θ between the incident light polarization and long axis of the AgNWs was also studied in this paper.

2. MATERIALS AND METHODS

2.1. Synthesis of MoS_2 and SERS Sample Preparation. The synthesis of MoS_2 on silica substrates was performed using a horizontal chemical vapor deposition (CVD) furnace with double temperature zones, which is depicted in the schematic diagram in Figure 1a. Before CVD growth, the silica substrate of 285 nm SiO_2 in thickness was cleaned using ultrasonication in acetone and ethanol, followed by annealing at 500 °C under an Ar atmosphere for 5 h. For the CVD growth of MoS_2, the silica substrate was placed face-down on top of a sample quartz boat in furnace 2 (Figure 1a). A source quartz boat loaded with sulfur powder (99.5%) was connected to a homemade putter and placed upstream in the heating zone 1 of furnace 1, next to the source quartz boat loaded with MoO_3 (99.99%) powder at the center of the heating zone. The optimal distance between S and Mo sources is around 10 cm. Prior to heating, the tube furnace was evacuated to approximately 100 mTorr with a vacuum pump and then filled with 100 sccm of ultrahigh purity argon gas (99.999%) to remove oxygen residues and other sources of contamination from air (5 min). Then, the two heating zones were heated to a certain temperature within 15 min (800 °C for MoO_3, 150 °C for S). When the temperature of the first heating zone reaches 150 °C, the S source was moved to the middle of the first heating zone to participate in the reaction by moving the magnet at the front of the putter. The reactants were kept at the set temperature for 15 min and then cooled naturally to room temperature. The Ar flow rate during the entire growth process was maintained as 75 sccm. During this process, the MoO_3 precursor was thermally evaporated from the quartz boat, reacted with S to form gaseous MoS_2 and diffuse across the boundary layer towards the growth substrate. Moreover, maintaining uniform melting/sublimation of the precursors and uniform vapor pressure of the gas-phase precursors are highly desirable for clean and reproducible growth of MoS_2.

The AgNWs were prepared using a solvothermal method.[20] The AgNWs were grown by reducing silver nitrate with ethylene glycol in the presence of poly(vinyl pyrrolidone). The ethylene glycol acts as both solvent and reducing agent. The prepared AgNWs with the diameter ranging from 200 to 400 nm were dispersed in ethanol and casted on MoS_2 flakes. To obtain the alignment of two AgNWs on a triangular MoS_2 flake, the AgNWs were manipulated using a fiber taper under an optical microscope. For the Raman study, a single droplet (~10 μL) of R6G anhydrous ethanol solution with a concentration of 1×10^{-6} M was casted on silica substrates with AgNWs and MoS_2 flakes. The polarization angle θ for Raman excitation was varied with respect to the axis of the aligned double AgNWs by rotating the sample stage to collect Raman spectra at selected θ angles.

2.2. Simulation of the Electromagnetic Field of Hybrid AgNWs–MoS_2 SERS Substrates. The simulation of the electromagnetic field distribution on the hybrid AgNWs–MoS_2 SERS substrates was carried out using a commercial Finite-difference Time Domain package (Lumerical Solutions, Inc.). The simulated model consisted of a single AgNW on a silica substrate covered with and without MoS_2 flake, respectively. The diameter of the AgNW was set at 300 nm and the thickness of MoS_2 was set at 1.5 nm. The wavelength of the excitation light was selected to be 532 nm. All simulations were performed using a mesh size of 0.2 nm in the x, y, and z directions. The dielectric functions of the AgNW and MoS_2 were taken, respectively, from Palik (1998)[21] and Hsu (2019).[22]

https://dx.doi.org/10.1021/acs.jpcc.0c08184
J. Phys. Chem. C 2021, 125, 1940–1946

2.3. Characterization. The morphology of the MoS_2 flakes was characterized using optical microscopy (Olympus, BX51M) and scanning electron microscopy (SEM, Hitachi, S-3400N). The morphology of the SERS samples was characterized using field-emission scanning electron microscopy (FESEM, JEOL, JSM-7800F). All Raman spectra and maps were measured using microscope imaging with a confocal Raman microscope (Thermo Fisher, DXR) under an incident laser wavelength at 532 nm with the power and beam spot diameter of 5 mW and 2 μm, respectively. It should be noted that a low laser power in the range of 1−5 mW is typically used for taking R6G Raman spectra to avoid molecular damages during the multiple scans during integration.[23]

3. DISCUSSION AND CONCLUSIONS

The optical image of the CVD grown MoS_2 flakes is shown in Figure 1b. All flakes exhibit triangular shapes, indicating the high-quality crystallinity of the MoS_2. The color contrast can be associated with the different thickness of MoS_2 flakes and the majority flakes with a deep blue contrast are monolayer MoS_2 flakes. Some multilayer MoS_2 flakes are also visible, and their dimension is smaller than their monolayer counterparts. The inset of Figure 1b is a zoom-in view of a monolayer MoS_2 flake, illustrating a nearly perfect triangular shape. The side length of the triangular monolayer MoS_2 flakes is in the range of a few microns to several tens of microns. The larger size of the MoS_2 flakes than that of the Raman laser spot size and AgNW's diameter is important because it allows for spatially resolved Raman spectroscopy on the hybrid AgNW−MoS_2 flake SERS substrates. Figure 1c shows the typical SEM image of the CVD MoS_2 flakes. It can be observed that most of the MoS_2 flakes are isolated islands with triangle-like morphologies because of the presence of an energetically preferred edge, that is, the zigzag edge.[24,25]

Figure 2 compares the Raman spectra of MoS_2 flakes excited by 532 nm laser under ambient conditions. Both E^1_{2g} (~384 cm^{-1} for monolayer MoS_2) and A_{1g} (~403 cm^{-1} for monolayer MoS_2) modes can be observed clearly in monolayer (1L), two-layer (2L), three-layer (3L), and bulk MoS_2. The E^1_{2g} mode mainly depends on the in-plane vibration of the two S atoms with respect to the Mo atom, and the A_{1g} mode is associated with the out-of-plane vibration of the S atoms in different layers,[26] as shown in the illustration in Figure 2. Besides, the presence of E^1_{2g} and A_{1g} modes indicates the formation of the 2H phase in both bulk and few-layer forms of MoS_2. Moreover, it can be observed that the frequency of the E^1_{2g} (A_{1g}) peak decreases (increases) monotonically, with the layer number increasing from 1 to 3. This is attributed to the variation of the interlayer van der Waals force in MoS_2 with the layer numbers.[27] However, for the bulk MoS_2, the red-shift of the E^1_{2g} mode can be attributed to the stacking-induced structure changes or long-range Coulombic interlayer interactions in MoS_2.[28]

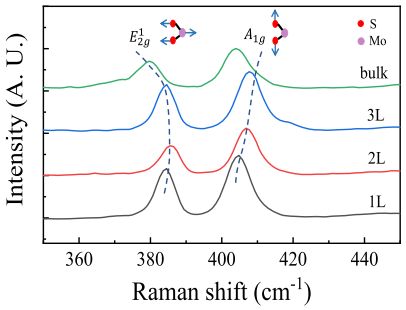

Figure 2. Raman spectra acquired in different layers of MoS_2 flakes under excitation of a 532 nm laser. The left and right dashed lines indicate the positions of the E^1_{2g} and A_{1g} peaks in MoS_2, respectively; the vibration modes of E^1_{2g} and A_{1g} are illustrated in the inset. "1 L", "2 L", and "3 L", respectively, indicate monolayer, bilayer, and trilayer for the MoS_2 flakes.

Figure 3 schematically shows the experimental setup for the Raman spectra measurement on the AgNWs−MoS_2 flake SERS substrates. To precisely contrast the differences of SERS performance between hybrid AgNWs−MoS_2 and aligned double AgNWs on cases, a half of the double AgNWs was placed on the MoS_2 flake, while the other half was placed on the silica substrate. The SERS enhancement of the two types of the substrates was investigated using standard R6G probe molecules. It is well known that the SERS has two mechanisms, namely, electromagnetic mechanism (EM) and chemical mechanism (CM).[29] The former is mainly attributed to the localized SPR of free charge carriers on the surface of metal nanostructures upon Raman excitation, which leads to enhancement of local electromagnetic fields around the metal structures such as the AgNWs in this work.[30] In addition, this localized evanescent field is affected not only by the dielectric environment of the AgNWs but also by the angle θ between the incident light polarization and the axis of the AgNWs. Thus, the SERS enhancement of the two types of the substrates with and without MoS_2 flakes was evaluated at three θ values of 0, 45, and 90° by rotating the sample.

Figure 4a and b compares the Raman spectra of R6G taken at θ = 0, 45, and 90° on the aligned double AgNWs SERS substrates without (Figure 4a) and with (Figure 4b) the MoS_2 flakes. At θ = 0° (black) for the sample without the MoS_2 flake (Figure 4a), the Raman signals of R6G are weak but visible at the peaks of 613 and 773 cm^{-1}, which, respectively, correspond to the in-plane bending mode of a C−C−C ring and C−H out-of-plane bending mode.[31] However, the Raman signals of R6G are greatly enhanced with the MoS_2 flake (Figure 4b), as illustrated in higher peak intensities at 613 and 773 cm^{-1} and more visible peaks of R6G at 1186 and 1572 cm^{-1} corresponding to the stretching vibrations for aromatic C−C. In fact, the same trend can be observed for the other two cases of θ = 45° (red) and 90° (blue), indicating that the presence of the MoS_2 flake near the AgNWs can considerably enhance the SERS effect of the AgNWs. It should be noted that two additional peaks belonged to MoS_2 at 382 cm^{-1} (E^1_{2g}) and 403 cm^{-1} (A_{1g}), respectively, are observed on the AgNW−MoS_2 samples. The frequency difference between the E^1_{2g} mode and the A_{1g} mode is around 21 cm^{-1}, indicating that the thickness of the MoS_2 flake in Figure 4 is bilayer.

Another interesting trend revealed in Figure 4 is that the Raman intensities of the R6G increase, with θ increasing from 0 to 90°, regardless of whether or not in the presence of MoS_2. This means that the Raman intensity is strongest when the polarization is perpendicular to the axis of the AgNWs. This is not surprising considering the dependence of the localized surface plasmon field of the AgNWs on the polarization of the Raman excitation.[32] The surface plasmon excitation efficiency is strongest when the incident light polarization is perpendicular to the long axis of the nanowires and lowest when parallel. In fact, we can observe a similar trend of the θ dependence of the Raman signal of the MoS_2 (Figure 4b). This

https://dx.doi.org/10.1021/acs.jpcc.0c08184
J. Phys. Chem. C 2021, 125, 1940−1946

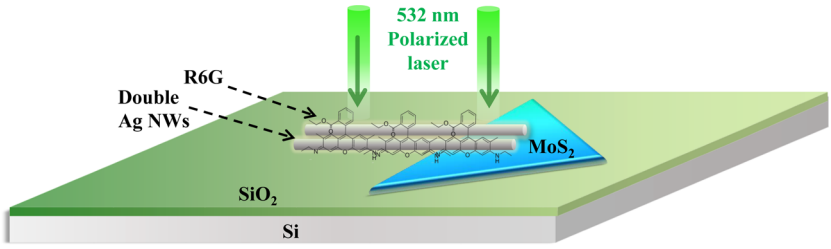

Figure 3. Schematic of the experiment on the R6G SERS measurements on double-aligned AgNWs with a half of NWs on a MoS_2 flake to form a hybrid Ag−MoS_2 SERS substrate and the other half on a bare silica substrate for comparison.

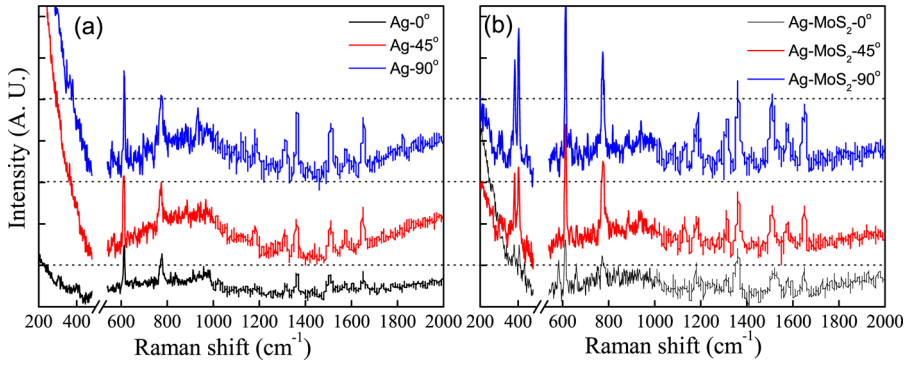

Figure 4. Raman spectra of R6G taken on (a) AgNWs and (b) hybrid AgNWs−MoS_2 SERS substrates.

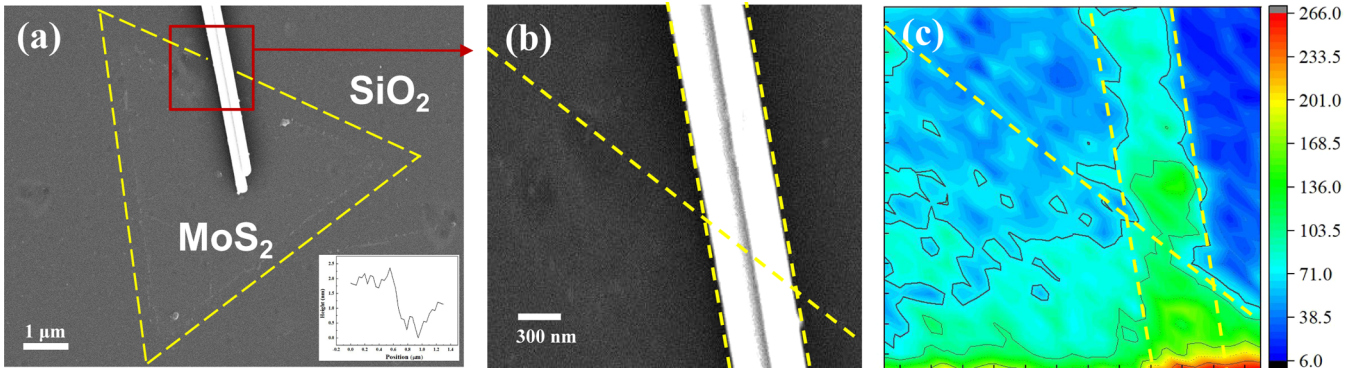

Figure 5. (a) SEM image of the SERS substrates consisting of double-aligned AgNWs with a half of NWs on a MoS_2 flake to form a hybrid MoS_2−AgNWs SERS substrate and the other half on a bare silica substrate for comparison. The yellow dotted line indicates the boundary of the MoS_2 flake. The inset picture is the thickness of the MoS_2 flake measured by AFM. (b) Enlarged SEM image corresponding to the marked red region in (a). (c) Raman map of the peak at 613 cm^{-1} of R6G under an excitation laser of 532 nm.

phenomenon can be attributed to the influence of the SERS of AgNWs on the MoS_2, as well as the case of R6G. Moreover, in order to quantitatively compare the SERS performance of the sample with and without MoS_2 under different θ, the enhancement factor β was defined by $\beta = I_{with}/I_{without}$, where I_{with} and $I_{without}$ are, respectively, the integration of all Raman peaks of R6G of the sample with and without the MoS_2 flake under certain θ. An enhancement factor β of 1.2, 1.5, and 1.7 can be achieved, respectively, for θ = 0, 45, and 90°, indicating the prominent effect of Ag−MoS_2 acting as a SERS substrate.

Figure 5 shows the SEM image and Raman maps of the sample. From the SEM image, double AgNWs with a diameter of 300 nm are observed with a side−by-side alignment. Moreover, as the yellow dashed line indicates, half of AgNWs are on the MoS_2 flake, while the other half are on the bare silica substrate. Because the thickness of the bilayer MoS_2 is relatively less, the color contrast between it and the silica substrate is not obvious, but it can be still seen from Figure 5a that the MoS_2 has a uniform thickness and regular triangular shape with a length 6 μm. Figure 5b is the partially enlarged view of the red rectangular frame marked in Figure 5a. The orange solid line in Figure 5b marks the side boundary of the MoS_2. To more clearly demonstrate the SERS effect, Figure 5c shows the 2D Raman maps of the mode intensity at 613 cm^{-1} of the R6G probe molecule, which was performed on the sample area of Figure 5b. The Raman intensity for the area of AgNWs−MoS_2 is highest in the mapping figure. Moreover, both the intensities at the exposed MoS_2 and AgNWs on silica substrate are higher than that of the bare substrate. Thus, Figure 5c obviously proves that the Ag−MoS_2 could significantly improve the SERS acting as an active substrate.

Although the MoS_2 may provide SERS enhancement based on the CM, we attribute the SERS mechanism observed in the hybrid AgNWs−MoS_2 in this work primarily to the EM. This argument is supported by the observed SPR on the double-aligned AgNWs (i.e., the EM) and the dependence of the

https://dx.doi.org/10.1021/acs.jpcc.0c08184
J. Phys. Chem. C 2021, 125, 1940−1946

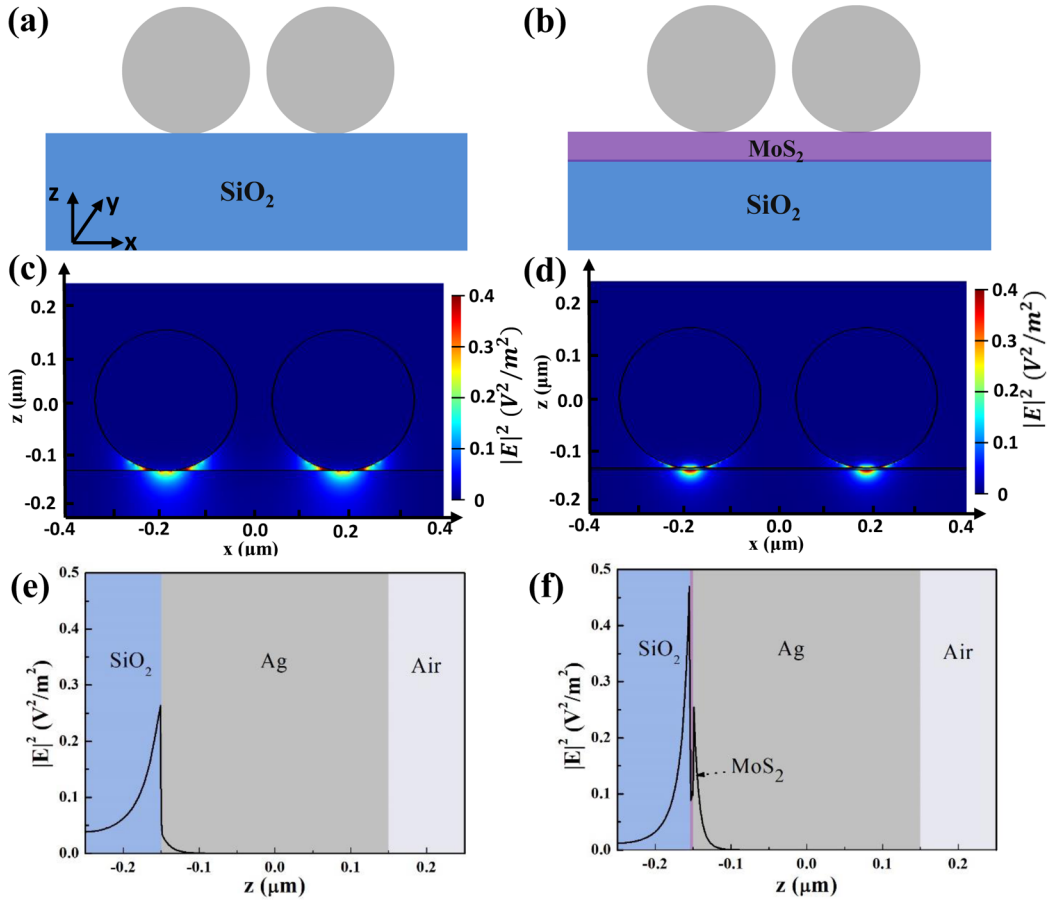

Figure 6. Cross sections of two AgNWs on substrates of (a) SiO_2 and (b) MoS_2/SiO_2. (c,d) are the simulated EM field variation in the *z*-axis for the two cases of (a,b), respectively. Circularly polarized light was used in the simulation. (e,f) are EM field intensities in the *z*-axis along the center of the cross section of the single Ag NW.

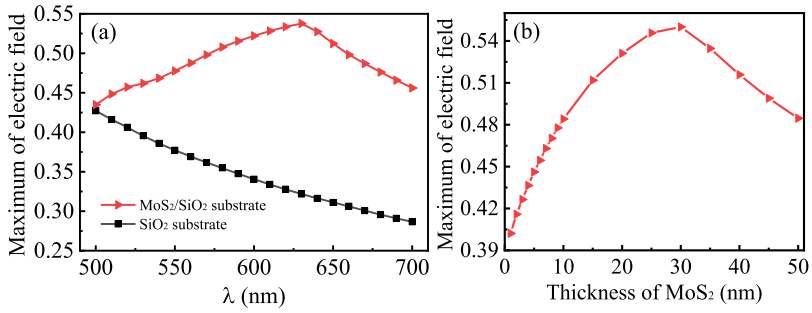

Figure 7. (a) Simulated maximum EM field ($|E|^2$) vs the Raman excitation wavelength. (b) Variation of the maximum EM field with the thickness of MoS_2.

Raman intensities of the R6G on the polarization orientation of the excited light with respect to the axial direction of the AgNWs. Moreover, the Raman signatures of the R6G at the site of the MoS_2 flake without Ag NWs are undetectable. In order to obtain some insights into the EM in the hybrid AgNWs−MoS_2 substrates, the localized electric fields of the AgNWs on the silica substrate were simulated under two conditions of with and without an MoS_2 flake. Figure 6a,b show the cross sections of the two models, while the electric field distributions and intensities of the models are present in Figure 6c−f. It is can be seen from Figure 6c,d that the MoS_2 layer on the silica substrate obviously affects the maximum electric field intensity around the AgNW. For the case with the MoS_2 layer, the electric field becomes more localized with an enhanced maximum electric field intensity. By contrasting the maximum electric field intensities under two conditions (Figure 6e,f), it can be concluded that the maximum electric field of AgNWs on MoS_2 is enhanced two times as compared to the case of AgNWs on the bare silica substrate. The localized electric field can act as a "hot spot" for SERS. As we all know, hot spots play an important role in SERS enhancement. For example, the adjacent site in the dimer of Ag NPs was confirmed to be the SERS hot spot using the combination of high-resolution transmission electron microscopic images and optical spectra of nanoparticle structures.[33] Moreover, this phenomenon was also confirmed by comparing the SERS intensity in a single Ag NP, and a dimer Ag NPs with a changed gap from 1.8 to 600 nm. Therefore, many efforts

https://dx.doi.org/10.1021/acs.jpcc.0c08184
J. Phys. Chem. C 2021, 125, 1940−1946

have been made in creating hot sites for SERS, such as NPs' trimers, chains, tips, or corners.[34,35] It is noted that there is no hot spot in the gap between the AgNWs in the present work because of the in-homogeneous dielectric environment of the surrounding materials of the AgNWs. In detail, for a homogeneous dielectric environment, there could be a hot spot in the gap between the two AgNWs. However, as the AgNWs are placed on a substrate, the distance of the surface plasmon coupling of the two AgNWs in the gap would shrink. Besides, the coupling distance is greatly reduced when the refractive index difference between the substrate and the covering material (air) is large. Thus, the original hot spot in the gap would disappear, and a new hot spot is formed in the interface site, where the refractive index of the surrounding material is largest.[36,37]

Moreover, the maximum intensity of the electric field changed with the excitation wavelength and the thickness of MoS_2 were also studied, as shown in Figure 7. It can be seen that the maximum electric field for the case with MoS_2 is larger than the case of the bare silica substrate in the range of 500−700 nm. For the case of the bare silica substrate, the maximum electric field shows linear decrease with the increase of the excitation wavelength. However, as the MoS_2 is introduced, the maximum electric field shows the different trend as compared with the case of silica substrate in the range from 500 to 630 nm and then presents an same trend when the wavelength further increases to 700 nm. Besides, the thickness of MoS_2 may also affect the maximum electric field intensity. Figure 7b presents the change of maximum electric field with the thickness of MoS_2 increasing from 0.63 nm (monolayer MoS_2) to 50 nm (bulk MoS_2). It can be seen that the maximum electric field increases with the thickness increasing from 0.63 to 30 nm, followed by a slight decline for the thickness larger than 30 nm.

In summary, we investigate the SERS performances of R6G probe molecules on the double-aligned AgNWs, half of which were placed on the bare silica substrate, while the other half were placed on a bilayer MoS_2 flake. As the results of Raman spectra and mapping indicated, the introduction of MoS_2 to AgNWs would enhance the Raman intensity of R6G than that of bare AgNWs. Moreover, this enhancement phenomenon is described by an enhancement factor β. It is found that the β is affected by the angle θ between the incident light polarization and long axis of the Ag NW, with the values of 1.2, 1.5, and 1.7, respectively, for θ = 0, 45, and 90°. Besides, both the Raman spectra intensities of R6G and MoS_2 are also influenced by the angle θ for both the cases of bare AgNWs and the Ag−MoS_2 hybrid structure. The present simulated results demonstrated that the enhancement of SERS in the hybrid AgNWs−MoS_2 nanostructure was largely attributed to the electric field enhancement of the hot spot at the interface between the Ag and MoS_2.

AUTHOR INFORMATION

Corresponding Authors

Liu Lu − *School of Mechanical Engineering, Jiangsu University, Zhenjiang 212013, China;* orcid.org/0000-0003-3691-646X; Email: lvliu@ustc.edu.cn

Judy Z. Wu − *Department of Physics and Astronomy, The University of Kansas, Lawrence 66044, United states;* Email: jwu@ku.edu

Authors

Lulu Yu − *School of Mechanical Engineering, Jiangsu University, Zhenjiang 212013, China*

Linghui Zeng − *School of Physical Sciences, University of Science and Technology of China, Hefei 230026, China*

Xiaohong Yan − *School of Mechanical Engineering, Jiangsu University, Zhenjiang 212013, China*

Xifeng Ren − *School of Physical Sciences, University of Science and Technology of China, Hefei 230026, China;* orcid.org/0000-0001-6559-8101

Complete contact information is available at: https://pubs.acs.org/10.1021/acs.jpcc.0c08184

Notes

The authors declare no competing financial interest.

ACKNOWLEDGMENTS

This work is funded by the National Natural Science Foundation of China (nos. 11204107 and 91750112). J.W. acknowledges supports from NSF contracts, NSF-DMR-1508494, NSF-ECCS-1809293, and NSF-DMR-1909292.

REFERENCES

(1) Mishra, A. K.; Mishra, S. K.; Verma, R. K. Graphene and Beyond Graphene MoS_2: A New Window in Surface-Plasmon-Resonance-Based Fiber Optic Sensing. *J. Phys. Chem. C* **2016**, *120*, 2893−2900.

(2) Shan, H.; Yu, Y.; Wang, X.; Luo, Y.; Zu, S.; Du, B.; Han, T.; Li, B.; Li, Y.; Wu, J. Direct observation of ultrafast plasmonic hot electron transfer in the strong coupling regime. *Light: Sci. Appl.* **2019**, *8*, 9.

(3) Li, Z.; Liu, C.; Rong, X.; Luo, Y.; Cheng, H.; Zheng, L.; Lin, F.; Shen, B.; Gong, Y.; Zhang, S.; Fang, Z. Tailoring MoS_2 valley-polarized photoluminescence with super chiral near field. *Adv. Mater.* **2018**, *30*, 1801908.

(4) Lin, Z.; Luo, P.; Zeng, W.; Lai, H.; Xie, W.; Deng, W.; Luo, Z. Improvement of photoelectric properties of MoS_2/WS_2 heterostructure photodetector with interlayer of Au nanoparticles. *Opt. Mater.* **2020**, *108*, 110191.

(5) Lee, B.; Liu, W.; Naylor, C. H.; Park, J.; Malek, S. C.; Berger, J. S.; Johnson, A. T. C.; Agarwal, R. Electrical tuning of exciton−plasmon polariton coupling in monolayer MoS_2 integrated with plasmonic nanoantenna lattice. *Nano Lett.* **2017**, *17*, 4541−4547.

(6) Chou, T.-M.; Chan, S.-W.; Lin, Y.-J.; Yang, P.-K.; Liu, C.-C.; Lin, Y.-J.; Wu, J.-M.; Lee, J.-T.; Lin, Z.-H. A highly efficient Au-MoS_2 nanocatalyst for tunable piezocatalytic and photocatalytic water disinfection. *Nano Energy* **2019**, *57*, 14−21.

(7) Peng, D.; Zhang, Y.; Xu, G.; Tian, Y.; Ma, D.; Zhang, Y.; Qiu, P. Synthesis of multilevel structured MoS_2@Cu/Cu_2O@C visible-light-driven photocatalyst derived from MOF−Guest polyhedra for cyclohexane oxidation. *ACS Sustainable Chem. Eng.* **2020**, *8*, 6622−6633.

(8) Wang, R.; Yan, X.; Ge, B.; Zhou, J.; Wang, M.; Zhang, L.; Jiao, T. Facile preparation of self-Assembled black phosphorus-dye composite films for chemical gas sensors and surface-enhanced Raman scattering performances. *ACS Sustainable Chem. Eng.* **2020**, *8*, 4521−4536.

(9) Wang, X.; Huang, S.-C.; Hu, S.; Yan, S.; Ren, B. Fundamental understanding and applications of plasmon-enhanced Raman spectroscopy. *Nat. Rev. Phys.* **2020**, *2*, 253−271.

(10) Mondal, S.; Subramaniam, C. Xenobiotic contamination of water by plastics and pesticides revealed through real-time, ultrasensitive, and reliable surface-enhanced raman scattering. *ACS Sustainable Chem. Eng.* **2020**, *8*, 7639−7648.

(11) Li, H.; Hu, W.; Hassan, M. M.; Zhang, Z.; Chen, Q. A facile and sensitive SERS-Based biosensor for colormetric detection of acetamiprid in green tea based on unmodified gold nanoparticles. *J. Food Meas. Charact.* **2019**, *13*, 259−268.

(12) Hassan, M. M.; Li, H.; Ahmad, W.; Zareef, M.; Wang, J.; Xie, S.; Wang, P.; Ouyang, Q.; Wang, S.; Chen, Q. Au@ Ag Nanostructure based SERS substrate for simultaneous determination of pesticides residue in tea via solid phase extraction coupled multivariate calibration. *LWT–Food Sci. Technol.* **2019**, *105*, 290−297.
(13) Lu, R.; Konzelmann, A.; Xu, F.; Gong, Y.; Liu, J.; Liu, Q.; Xin, M.; Hui, R.; Wu, J. Z. High sensitivity surface enhanced Raman spectroscopy of R6G on in situ fabricated Au nanoparticle/graphene plasmonic substrates. *Carbon* **2015**, *86*, 78−85.
(14) Su, S.; Zhang, C.; Yuwen, L.; Chao, J.; Zuo, X.; Liu, X.; Song, C.; Fan, C.; Wang, L. Creating SERS hot spots on MoS_2 nanosheets with in situ grown gold nanoparticles. *ACS Appl. Mater. Interfaces* **2014**, *6*, 18735−18741.
(15) Qiu, H.; Wang, M.; Li, L.; Li, J.; Yang, Z.; Cao, M. Hierarchical MoS_2-Microspheres decorated with 3D AuNPs arrays for high-efficiency SERS sensing. *Sens. Actuators, B* **2018**, *255*, 1407−1414.
(16) Singha, S. S.; Mondal, S.; Bhattacharya, T. S.; Das, L.; Sen, K.; Satpati, B.; Das, K.; Singha, A. Au nanoparticles functionalized 3D-MoS_2 nanoflower: An efficient SERS matrix for biomolecule sensing. *Biosens. Bioelectron.* **2018**, *119*, 10−17.
(17) Chen, P. X.; Qiu, H. W.; Xu, S. C.; Liu, X. Y.; Li, Z.; Hu, L. T.; Li, C. H.; Guo, J.; Jiang, S. Z.; Huo, Y. Y. A novel surface-enhanced Raman spectroscopy substrate based on a large area of MoS_2 and Ag nanoparticles hybrid system. *Appl. Surf. Sci.* **2016**, *375*, 207−214.
(18) Zu, S.; Li, B.; Gong, Y.; Li, Z.; Ajayan, P. M.; Fang, Z. Active control of plasmon−exciton coupling in MoS_2−Ag hybrid nanostructures. *Adv. Opt. Mater.* **2016**, *4*, 1463−1469.
(19) Li, Z.; Shegai, T.; Haran, G.; Xu, H. Multiple-Particle nanoantennas for enormous enhancement and polarization control of light emission. *ACS Nano* **2009**, *3*, 637−642.
(20) Lu, L.; Tong, X.; Zhang, X.; Ren, N.; Jiang, B.; Lu, H. Hot spot assisted blinking suppression of CdSe quantum dots. *Chem. Phys. Lett.* **2016**, *652*, 167−171.
(21) Palik, E. D. *Handbook of Optical Constants of Solids*; Academic Press, 1998; p 3.
(22) Hsu, C.; Frisenda, R.; Schmidt, R.; Arora, A.; Vasconcellos, S. M.; Bratschitsch, R.; Zant, H. S. J.; Castellanos-Gomez, A. Thickness dependent refractive index of 1L, 2L, and 3L MoS_2, $MoSe_2$, WS_2, and WSe_2. *Adv. Opt. Mater.* **2019**, *7*, 1900239.
(23) Ghopry, S. A.; Alamri, M.; Goul, R.; Cook, B.; Sadeghi, S. M.; Gutha, R. R.; Sakidja, R.; Wu, J. Z. Au Nanoparticle/WS_2 Nanodome/Graphene Van Der Waals Heterostructure Substrates for Surface-Enhanced Raman Spectroscopy. *ACS Appl. Nano Mater.* **2020**, *3*, 2354−2363.
(24) Wang, S.; Rong, Y.; Fan, Y.; Pacios, M.; Bhaskaran, H.; He, K.; Warner, J. H. Shape evolution of monolayer MoS_2 crystals grown by chemical vapor deposition. *Chem. Mater.* **2014**, *26*, 6371−6379.
(25) Zhang, W.; Li, X.; Jiang, T.; Song, J.; Lin, Y.; Zhu, L.; Xu, X. CVD synthesis of $Mo_{(1-X)}W_XS_2$ and $MoS_{2(1-X)}Se_{2X}$ alloy monolayers aimed at tuning the bandgap of molybdenum disulfide. *Nanoscale* **2015**, *7*, 13554−13560.
(26) Majee, B. P.; Mishra, S.; Pandey, R. K.; Prakash, R.; Mishra, A. K. multifunctional few-layer MoS_2 for photodetection and surface-enhanced Raman spectroscopy application with ultrasensitive and repeatable detectability. *J. Phys. Chem. C* **2019**, *123*, 18071−18078.
(27) Bagnall, A. G.; Liang, W. Y.; Marseglia, E. A.; Welber, B. Raman studies of MoS_2 at high pressure. *Physica B+C* **1980**, *99*, 343−346.
(28) Lee, C.; Yan, H.; Brus, L. E.; Heinz, T. F.; Hone, J.; Ryu, S. Anomalous lattice vibrations of single-and few-layer MoS_2. *ACS Nano* **2010**, *4*, 2695−2700.
(29) Otto, A. Surface-enhanced Raman scattering of adsorbates. *J. Raman Spectrosc.* **1991**, *22*, 743−752.
(30) Lu, L.; Tan, R.; Chen, D.; Tong, Y.; Yan, X.; Gong, M.; Wu, J. Z. Surface plasmon assisted laser ablation of stainless steel. *Nanotechnology* **2019**, *30*, 305401.
(31) Majee, B. P.; Srivastava, V.; Mishra, A. K. Surface-enhanced Raman scattering detection based on an interconnected network of vertically oriented semiconducting few-layer MoS_2 nanosheets. *ACS Appl. Nano Mater.* **2020**, *3*, 4851−4858.
(32) Lu, L.; Wang, L.-L.; Zou, C.-L.; Ren, X.-F.; Dong, C.-H.; Sun, F.-W.; Yu, S.-H.; Guo, G.-C. doubly and triply coupled nanowire antennas. *J. Phys. Chem. C* **2012**, *116*, 23779−23784.
(33) Nie, S.; Emory, S. R. Probing single molecules and single nanoparticles by surface-enhanced Raman scattering. *Science* **1997**, *275*, 1102−1106.
(34) Svedberg, F.; Li, Z.; Xu, H.; Käll, M. Creating hot nanoparticle pairs for surface-enhanced Raman spectroscopy through optical manipulation. *Nano Lett.* **2006**, *6*, 2639−2641.
(35) Ding, S. Y.; Yi, J.; Li, J. F.; Ren, B.; Wu, D. Y.; Panneerselvam, R.; Tian, Z. Q. Nanostructure-based plasmon-enhanced Raman spectroscopy for surface analysis of materials. *Nat. Rev. Mater.* **2016**, *1*, 16021.
(36) Xiong, X.; Zou, C.-L.; Ren, X.-F.; Liu, A.-P.; Ye, Y.-X.; Sun, F.-W.; Guo, G.-C. Silver nanowires for photonics applications. *Laser Photonics Rev.* **2013**, *7*, 901−919.
(37) Lu, L.; Zhang, X.; Tong, X.; Xu, X. F.; Ren, N. F. Investigating several surface plasmon characteristics dependent on the surrounding dielectric environment, Optoelectron. *Adv. Mater.* **2015**, *9*, 1180−1184.

https://dx.doi.org/10.1021/acs.jpcc.0c08184
J. Phys. Chem. C 2021, 125, 1940−1946